Collision Dynamics of Argon Cluster Ions, Ar^+_n (n=3-23) : Molecular Dynamics Simulation Based on Diatomics-in-Molecules Method

Sci. Rep. RITU A41 (1996) pp. 191-195
No. 2, January 1996

Collision Dynamics of Argon Cluster Ions, Ar_n^+ ($n = 3-23$): Molecular Dynamics Simulation Based on Diatomics-in-Molecules Method

Masahiko Ichihashi [a], Tsutomu Ikegami [b] and Tamotsu Kondow [a]

[a] *Department of Chemistry, School of Science, The University of Tokyo, Bunkyo-ku, Tokyo 113, Japan*
[b] *Institute for Molecular Science, Myodaiji, Okazaki, Aichi 444, Japan*

(Received November 14, 1995)

The molecular dynamics method combined with a quantum mechanical calculation has been used to simulate the collision between an argon atom and an argon cluster ion, Ar_n^+ ($n = 3-23$), which contains a given amount of internal energy. Two pathways were observed; (i) Evaporation after collisional energy transfer to the internal degrees of freedom *vs.* (ii) fusion via complex formation. The total reaction cross sections were compared with those experimentally obtained. It is found that the branching fractions of the evaporation and the fusion depend critically on the internal energy and the impact parameter.

KEYWORDS: Ar_n^+, collision-induced dissociation, molecular dynamics, diatomics-in-molecules method

1. Introduction

Collision-induced reactions between cluster ions and molecules have been investigated extensively[1-9], since the results provide useful information on the structures and reactions of the cluster ions. On the other hand, simulations have been performed to obtain more detailed information about the dynamics of the collisional dissociation[10-13]. Stace and co-workers have examined a pick-up reaction of Ar_{20} with CH_3CN by use of a molecular dynamics (MD) method[11]. They have found that in a head-on collision the cluster melts immediately, and the projectile CH_3CN molecule rests on the cluster surface and then migrates into the melting cluster within ≈ 40 ps. P. de Pujo *et al.* have studied 0.2-eV collision of a rare gas atom, He, Ar or Xe, with Ar_{125}[12]. It has been found that the He atom is only deflected by the cluster, while the Ar or Xe atom is captured in it. In the Xe-collision, the captured projectile migrates inside the cluster because the collision gives causes the cluster to melt. In a system containing a charged particle, collision dynamics is slightly different. Attachment of a Xe^+ ion with a thermal energy to Ar_{29} has been simulated by an MD method[13]. The Xe^+ projectile ion is pulled quickly into the center of the cluster wherever the collision takes place. They have suggested that (i) the incoming projectile ion gains a momentum on an attractive potential energy surface, (ii) the cluster is more stable when the ion core, Xe^+, is in the center of the cluster and (iii) the structure of the cluster is loosened due to melting of the cluster. These studies have demonstrated that the collision dynamics can be well visualized.

A classical MD method has a limitation to deal with charged cluster since the charge distribution changes with changing the geometry of the clusters through strong electron-phonon coupling. In an argon cluster ion, Ar_n^+, the positive charge is delocalized among three argon atoms in its electronic ground state, while the charge distribution changes significantly with the geometry change through its strong electron-phonon interaction[14-17]. Experimental studies on the collisional dissociation of Ar_n^+ with Kr[5] also indicate that such classical MD calculations are not adequate; Kr atoms react with the ion core of Ar_n^+ to form $ArKr^+$.

In the present report, we described a quantum molecular dynamics simulation to investigate one of the most fundamental collisional processes,

$$\mathrm{Ar} + \mathrm{Ar}_n^+ \begin{cases} \nearrow \\ \searrow \end{cases} \begin{array}{ll} \mathrm{Ar} + \mathrm{Ar}_n^{+\dagger} & \rightarrow \quad \mathrm{Ar}_{n'}^+ + (n-n')\mathrm{Ar} + \mathrm{Ar} \\ & \qquad \text{(Evaporation)} \\ [\mathrm{ArAr}_n]^{+\dagger} & \rightarrow \quad \mathrm{ArAr}_{n'-1}^+ + (n-n'+1)\mathrm{Ar} \\ & \qquad \text{(Fusion),} \end{array} \tag{1}$$

The results are compared with our previous experimental results[6] on the absolute cross sections for the collisional evaporation of Ar_n^+ and for the formation of a fused cluster ion, $^{36}ArAr_{n'-1}^+$.

2. Calculation

The simulation of the collision event between Ar_n^+ and Ar was performed by use of a molecular dynamics (MD) method combined with the diatomics-in-molecules (DIM) method. As this method has been reported in a previous paper in detail[16], a brief explanation is given here. In the DIM method[17], the Hamiltonian is given by the sum of the atomic and the diatomic Hamiltonians,

$$\mathcal{H} = \sum_{A>B}^{n} \mathcal{H}^{AB} - (n-2)\sum_{A}^{n} \mathcal{H}^{A}, \tag{2}$$

where A and B denote atoms in a cluster and $\mathcal{H}^A$ and $\mathcal{H}^{AB}$ represent the atomic and the diatomic Hamiltonians, respectively, and n is the number of atoms in the cluster ion, Ar_n^+. Equation (2) enables us to construct the total Hamiltonian matrix from the atomic and the diatomic Hamiltonian matrices. Then the Hamiltonian matrices for Ar, Ar^+, Ar_2 and Ar_2^+ are indispensable to obtain the matrix elements for Ar_n^+. The wave function, Ψ_g, of the electronic ground state of the cluster ion can

be expanded by a set of appropriate basis functions:

$$\Psi_g = \sum_A^n \sum_{w=x,y,z} c_A^w \psi_A^w, \tag{3}$$

$$\psi_A^w = S_1 S_2 S_3 \cdots P_A^w \cdots S_n, \tag{4}$$

where S_i and P_A^w represent the wave functions for the Ar atoms and the Ar^+ having a hole on the $3p_w$ orbital, respectively. Within the DIM framework, the orthonormality of the basis functions is premised to be valid. The matrix elements of $\mathcal{H}^C$ and $\mathcal{H}^{CD}$ are given by,

$$\langle \psi_A^w | \mathcal{H}^C | \psi_B^v \rangle = \delta_{AB}\delta_{wv}(1-\delta_{AC})(-\mathrm{IP(Ar)}) \tag{5}$$

$$\langle \psi_A^w | \mathcal{H}^{CD} | \psi_B^v \rangle = \begin{cases} H^{AB}_{Aw,Bv}(r_{AB};\mathrm{Ar}_2^+) & \{A,B\} \equiv \{C,D\} \\ \delta_{AB}\delta_{wv}E(r_{CD};\mathrm{Ar}_2) & \{A,B\} \cap \{C,D\} = \emptyset \\ 0 & \text{otherwise,} \end{cases} \tag{6}$$

where IP(Ar), $H^{AB}_{Aw,Bv}(r_{AB};\mathrm{Ar}_2^+)$ and $E(r_{CD};\mathrm{Ar}_2)$ represent the ionization potential of an Ar atom, the Hamiltonian matrix elements of Ar_2^+ and the potential energy of Ar_2, respectively, and r_{AB} is the distance between A and B.

The energy, E_g, of the electronic ground state is given by,

$$E_g = \langle \Psi_g | \mathcal{H} | \Psi_g \rangle = \sum_i \sum_j c_i^* c_j H_{ij}, \tag{7}$$

where i denotes A and w, and H_{ij} represents the ij matrix element of the total Hamiltonian, $\mathcal{H}$. The force, $\vec{F}$, is given by,

$$\vec{F} = -\vec{\nabla} E_g \tag{8}$$

$$= -\sum_i \sum_j c_i^* c_j \vec{\nabla} H_{ij}. \tag{9}$$

The steepest decent method was employed to find the most stable structure by using the potential gradients given by eqs.(8) and (9). A known amount of internal energy, E, was given to a parent cluster ion, Ar_n^+, at 0 K. The internal temperature of the cluster ion turns out to be,

$$T = \frac{E}{(3n-6)k_B}, \tag{10}$$

where k_B represents the Boltzmann constant. A projectile, Ar atom, was placed initially at 50 Å apart from the center-of-mass of Ar_n^+ possessing the internal energy of E, and was allowed to collide with the Ar_n^+ at a given impact parameter and relative velocity. The initial position of the projectile was given at random, with positioning Ar_n^+ having an averaged orientation. The impact parameter was chosen so as to cover a circle uniformly with the radius of b_0, which is typically 10 Å. The Newtonian equations of motion of Ar atoms were integrated by the fourth order predictor-fifth order corrector method. The time step is 100 a.u. (= 2.4189 fs), so that the total energy was maintained within the variance of less than 0.05% throughout the calculation. The collision events were simulated in the short time range (30 ps) and the long time range (800 ps), and simulations of the short time range were repeated more than 100 times. The reaction cross section, σ, was calculated by the following equation:

$$\sigma = \frac{N_r}{N}\pi b_0^2, \tag{11}$$

where N and N_r represent the number of the total runs of MD and the number of the runs which leads to the reactions, respectively, and b_0 represents the maximum impact parameter employed.

3. Results

The projectile Ar atom separated by 50 Å from the target cluster ion, Ar_{13}^+, at $t = 0$ collides with Ar_{13}^+ at $t \approx 5$ ps for the 0.2-eV collision. Several simulations of collision events were performed for 800 ps and two typical processes were observed.

(i) In a typical evaporation process, the projectile Ar atom was deflected with leaving vibrationally excited Ar_{13}^+. At $t = 29$ ps, one Ar atom was ejected from Ar_{13}^+. The remainder, Ar_{12}^+, was still vibrationally hot and at $t = 522$ ps, one more Ar atom was ejected. After all, during 800 ps, Ar_{13}^+ was found to release two Ar atoms and Ar_{11}^+ was produced.

(ii) In a typical fusion process, the projectile Ar atom was captured by Ar_{13}^+ and the complex cluster ion, $ArAr_{13}^+$, was produced. During the next following 18 ps, it was vibrationally excited and at $t = 23$ ps one Ar atom was ejected. The remainder, $ArAr_{12}^+$, having much internal energy released one more Ar atom at $t = 148$ ps; more Ar atoms were released sequentially at later times. Finally, Ar_{13}^+ became $ArAr_{10}^+$. In this case, the energy brought by the projectile Ar atom is completely randomized so that the projectile Ar atom is no more distinguished from the other Ar atoms.

These collisional processes are given in eq.(1). In general, the intermediate cluster ions, $Ar_n^{+\dagger}$ and $[ArAr_n]^{+\dagger}$, are produced at $t \approx 5$ ps.

Figure 1 shows the size-distribution of the daughter ions at $t = 30$ ps in the 0.2-eV collision of Ar_{13}^+ with an Ar atom. At 0 K, $ArAr_{13}^+$ is the most abundant daughter ion. Namely, the fusion pathway proceeds much more efficiently. At 50 K, $ArAr_{13}^+$, $ArAr_{12}^+$ and $ArAr_{11}^+$ are produced via the fusion pathway in addition to Ar_{12}^+ through the evaporation pathway. For internal temperatures up to 100 K, $ArAr_{11}^+$ and $ArAr_{10}^+$ become the dominant daughter ions in addition to much more abundant Ar_{11}^+ and Ar_{10}^+. The evaporation pathway proceeds much more rapidly than the fusion one.

The distributions of the daughter ions at $t = 30$ ps are not similar to the measured distribution of the product ions[6]. In the experiment, the product ions, $Ar_{n'}^+$, via the evaporation pathway distribute from $n' = 5$ to 12. The temperature of the parent cluster ion, Ar_{13}^+, is estimated to be 50 K from the result of unimolecular dissociation in the experiment. There is a significant difference between the calculated and the experimentally obtained distributions. This is explained from the viewpoint of

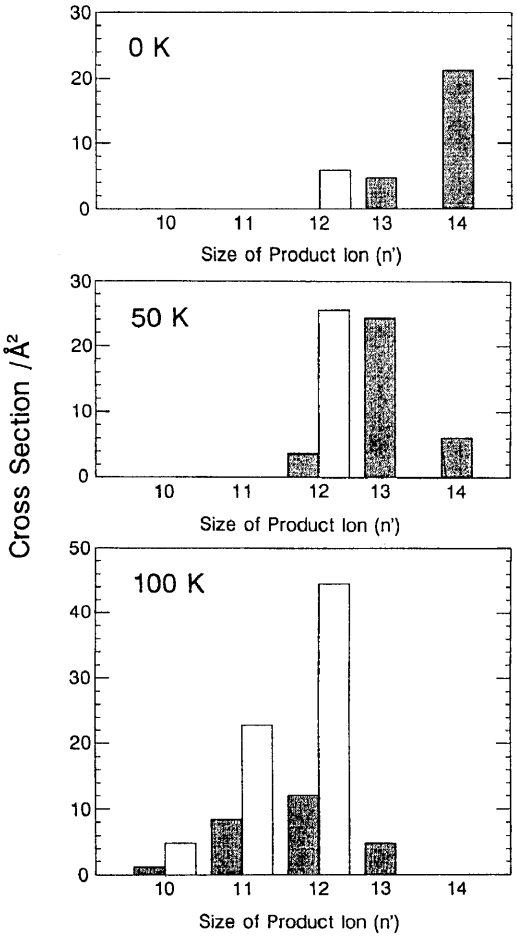

Figure 1. Size-distributions of the daughter ions at $t = 30$ ps at the 0.2-eV collision between Ar_{13}^+ and an Ar atom. The initial internal temperature is 0 K, 50 K and 100 K, respectively. The white histograms represent $Ar_{n'}^+$ produced by the evaporation, and the shaded ones represent $Ar^*Ar_{n'-1}^+$ produced by the fusion. Ar^* denotes the projectile atom.

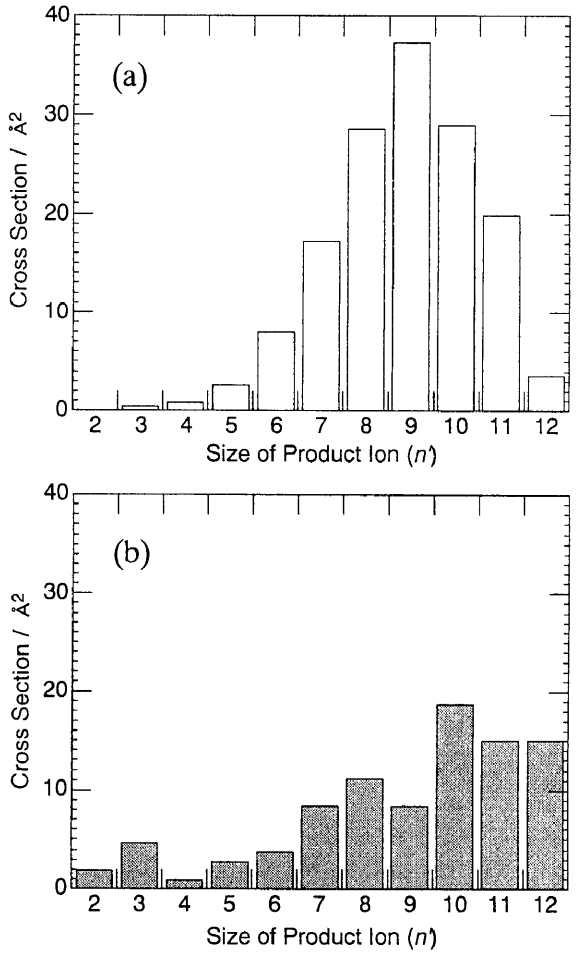

Figure 2. Cross sections for the production of cluster ions produced by evaporation in the collision of Ar_{13}^+ with an Ar atom at the collision energies of 2.0 eV; the experimental cross sections [panel (a)] *vs.* the simulation [panel (b)].

the dissociation rate. If the energy acquired by the collision is independent of the initial internal energy of the parent cluster ion, Ar_{13}^+ at 100 K has the largest amount of total internal energy after the collision. The cross section for the production of the daughter ion at $t = 30$ ps depends on the dissociation rate of the parent cluster ion. Thus the total cross section seems to increase with the initial internal temperature, because the dissociation rate increases with the total internal energy.

Actually, the distributions for the 2.0-eV collision become relatively similar to each other because of the high dissociation rate. Figure 2 shows the calculated and the measured distributions of the product ions via the evaporation pathway. In the experiment, the product ions, $Ar_{n'}^+$, distribute from $n' = 3$ to 12, and Ar_9^+ is the most abundant product ion. In the simulation, the product ions, $Ar_{n'}^+$, distribute from $n' = 2$ to 12 and Ar_{10}^+ is the most abundant product ion. This calculated distribution reproduces the measured one fairly well. The cross section for the fusion pathway is calculated to be 5.6 $Å^2$ in agreement with the observed cross section of 8.43 $Å^2$.

The reaction cross sections for the 2.0 eV collision can be calculated if this simulation is continued until several hundred microseconds. As the long-time simulation is not practically feasible, the cross sections were estimated by taking advantage of the relation between the impact parameter and the collisional excitation energy. Figure 3 shows the kinetic energy loss of the projectile Ar atom in the center-of-mass frame as a function of the impact parameter. This kinetic energy loss gives the energy acquired by the parent cluster ion, Ar_{13}^+, at the 0.2-eV collision. When the impact parameter is larger than 7 Å, the kinetic energy loss becomes almost zero. This result shows that the maximum distance for the appreciable interaction between Ar_{13}^+ and the projectile Ar atom is about 7 Å. The cluster ions with other sizes ($n = 3-23$) were treated in the same way.

4. Discussion

When Ar_n^+ is regarded as a hard sphere, the kinetic energy loss of the projectile Ar atom is given by the following equation in the cluster-fixed laboratory frame as a function of the impact parameter, b:

$$E_{HS} = \frac{4Mm}{M+m}\left\{1-\left(\frac{b}{R+r}\right)^2\right\}E_{LAB}, \qquad (12)$$

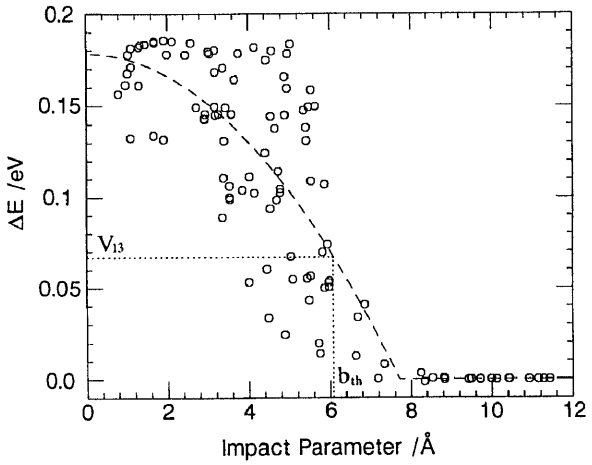

Figure 3. Kinetic energy loss of the projectile Ar atom at the 0.2-eV collision of Ar_{13}^+ as a function of the impact parameter, b. The internal temperature of Ar_{13}^+ is 50 K. The dashed curve is the theoretical curve calculated from a classical collision model (see text).

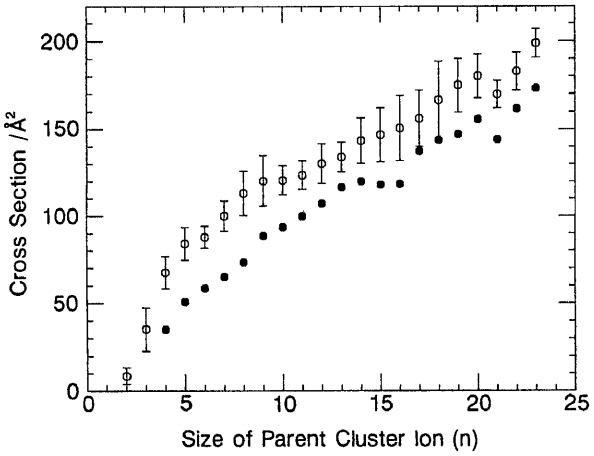

Figure 4. Total cross sections by the experiment (○) and the simulation (●) at collision energy of 0.2 eV.

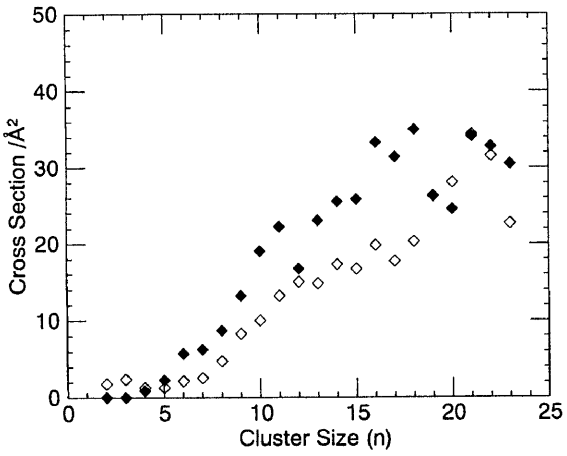

Figure 5. Fusion cross sections by the experiment (◇) and the simulation (◆) at collision energy of 0.2 eV.

where $E_{\rm LAB}$ indicates the collision energy in the laboratory frame, M and m represent the masses of Ar_n^+ and an Ar atom respectively, and R and r represent the radii of Ar_n^+ and an Ar atom, respectively. In the hard sphere model, $E_{\rm HS}$ is the translational energy of Ar_n^+ after the collision. Actually, Ar_n^+ has the internal degrees of freedom and most of $E_{\rm HS}$ transfers to the intracluster vibrational modes of Ar_n^+. The increment of the internal energy, ΔE, by the collision is estimated as follows:

$$\Delta E = \Gamma E_{\rm CM}\left\{1-\left(\frac{b}{R+r}\right)^2\right\}, \qquad (13)$$

where $E_{\rm CM}$ and Γ represent the collision energy in the center-of-mass frame and energy-conversion efficiency from the collision energy to the internal one, respectively. The dashed curve in Fig.3 was obtained by use of the least square fitting of eq.(13) to the calculated plots. In the 0.2-eV collision between Ar_{13}^+ and an Ar atom, the values of Γ and $b_{\rm max}$ $(= R + r)$ are 0.89 and 7.7 Å. The averaged increment of the internal energy is 90 meV, which gives rise to the internal temperature of 30 K by use of eq.(10). The bond dissociation energy of Ar_{12}^+–Ar (V_{13}) is estimated to be 0.0671 eV from that of Ar_{10}^+–Ar[18]. When ΔE is larger than this value, the parent cluster ion can dissociate. The total reaction cross section is estimated to be 120 $Å^2$ from this opacity function. This value is almost equal to the cross section obtained experimentally (134 $Å^2$). However, the experimental value is a little larger than the calculated one. Figure 4 shows the total reaction cross sections obtained from the experiment and estimated from this simulation. By using the same bond dissociation energies of Ar_{n-1}^+–Ar as those used in the analysis of experimental results in the previous paper[6], one obtains the cross sections, which agree with the experimental cross sections. The slightly smaller calculated cross sections suggest that Ar_n^+ may be dissociated even when the excitation energy is less than the bond dissociation energy, because of a finite amount of its initial internal energy. A small kink around $n = 13$ in the n-dependence of the cross section and the slope between $n = 13$ and 14 confirms that the geometrical shell closes at $n = 13$. This simulation also reproduces the sudden decrease of the cross section at $n = 21$, since Ar_{21}^+ has the more closely packed structure than Ar_{20}^+ has. In the most stable structure of Ar_{20}^+, an additional atom is attached to Ar_{19}^+ in the second solvation shell. On the other hand, in Ar_{21}^+, two additional atoms start to form a new cap at the open end of the ion core of Ar_{19}^+[16].

Figure 5 shows the fusion cross sections in comparison with the experimental ones. The fusion cross section, $\sigma_{\rm f}$, in this simulation was estimated by the following equation,

$$\sigma_{\rm f} = \left(1-\frac{{}_nC_2}{{}_{n+1}C_3}\right)\frac{1}{N}\sum_i^N \theta_i, \qquad (14)$$

where θ_i is set to be unity if the cluster ion contains the projectile Ar atom in the i-th trajectory at $t = 30$ ps and otherwise θ_i is zero. The prefactor, $1 - {}_nC_2/{}_{n+1}C_3$,

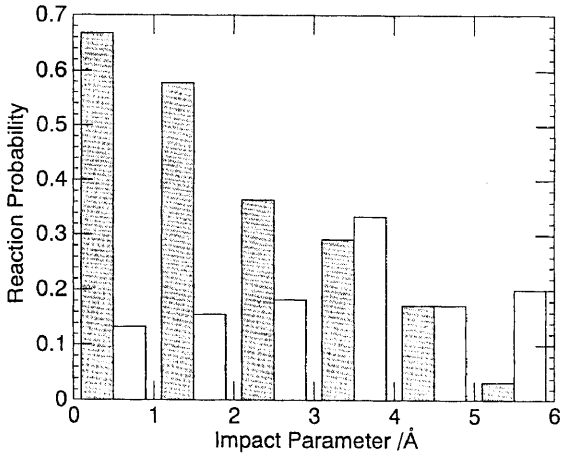

Figure 6. Reaction probabilities of Ar_{13}^+ at the 0.2-eV collision. The white and the shaded histograms represent those for the evaporation and fusion pathways, respectively.

shows the probability that the cluster, $[ArAr_n^+]^\dagger$, does not release the projectile Ar atom. As $[ArAr_n^+]^\dagger$ is supposed to have available energy of 0.2 eV because of the perfectly inelastic collision, $[ArAr_n^+]^\dagger$ can release three Ar atoms energetically. The calculated fusion cross sections are about 1.5 times larger than those experimentally obtained. However, the calculated fusion cross section reproduces the rapid rise around $n = 7$ and the tendency of leveling off around $n = 13$. The reason of the difference attributes to the initial internal energy of the parent cluster ion. The cross sections of the fusion pathway appears to change sensitively with the internal temperature of parent cluster ion (see Fig.1). This sensitiveness may bring a sizable error to the calculation.

In Fig.6, we show the probabilities of the evaporation and the fusion pathways as a function of the impact parameter for the system $Ar_{13}^+ + Ar$. This result shows that in the collision with the impact parameter of less than $\approx$ 2 Å, the fusion pathway dominates. As the impact parameter increases, the probability for the fusion pathway rapidly decreases and in turn the evaporation pathway supersedes the fusion one. In the fusion pathway, several events occurs independently in the vibrationally excited cluster ion, $[ArAr_n]^{+\dagger}$; release of Ar atoms from $[ArAr_n]^{+\dagger}$, exchange of the atoms in the ion core with the others, and the charge delocalization outside the ion core. In the fusion trajectories of about 15%, the projectile Ar atom has a positive charge more than 0.1 for $n = 13$. Note that the linear trimer core ion of Ar_{13}^+ in the ground state has the positive charges of 0.5 and 0.25 at the central and the outer two Ar atoms, respectively[16]. In the vibrationally excited $[ArAr_n]^{+\dagger}$, the positive charge is extended among the Ar atoms in the first solvation shell, and effectively, Ar_2^+, Ar_4^+ etc. are produced temporally. The probability that the projectile Ar atom is positively charged more than 0.1 is suppressed to less than $\approx$ 3% above $n = 14$. This suggests that the projectile Ar atom can not reach the ion core easily because the completed solvating shell prevents the projectile Ar atom from colliding directly with the ion core.

Acknowledgements

The authors acknowledge stimulating discussion with Prof. K. Someda and Dr. J. Hirokawa. Thanks are also due to the University of Tokyo Meson Science Laboratory (UTMSL) for the use of the TKYVAX computer. One of the authors (MI) is awarded the fellowship of the Japan Society for the Promotion of Science for Japanese Young Scientists.

1) P. A. Hints, M. B. Sowa, S. A. Ruatta and S. L. Anderson: J. Chem. Phys. **94** (1991) 6446.
2) S. A. Ruatta, P. A. Hints and S. L. Anderson: J. Chem. Phys. **94** (1991) 2833.
3) S. K. Loh, D. A. Hales, L. Lian and P. B. Armentrout: J. Chem. Phys. **90** (1989) 5466.
4) S. K. Loh, L. Lian and P. B. Armentrout: J. Am. Chem. Soc. **111** (1989) 3167.
5) M. Ichihashi, J. Hirokawa, S. Nonose, T. Nagata and T. Kondow: Chem. Phys. Lett. **204** (1993) 219.
6) M. Ichihashi, S. Nonose, T. Nagata and T. Kondow: J. Chem. Phys. **100** (1994) 6458.
7) J. Hirokawa, M. Ichihashi, S. Nonose, T. Tahara: T. Nagata and T. Kondow, J. Chem. Phys. **101** (1994) 6625.
8) C. A. Woodward and A. J. Stace: J. Chem. Phys. **94** (1991) 4234.
9) E. E. B. Campbell, R. R. Schneider, A. Hielscher, A. Tittes, R. Ehlich and I. V. Hertel: Z. Phys. D **22** (1992) 521.
10) M. Ichihashi, Y. Ozaki and T. Kondow: Chem. Phys. Lett. **198** (1992) 353.
11) G. Del Mistro and A. J. Stace: Chem. Phys. Lett. **196** (1992) 67.
12) P. de Pujo, J. -M. Mestgagh, J. -P. Visticot, J. Cuvellier, P. Meynadier, O. Sublemontier, A. Lallement and J. Berlamde: Z. Phys. D **25** (1993) 357.
13) M. Kolibiar, M. Foltin and T. D. Märk: Chem. Phys. Lett. **219** (1994) 252.
14) N. E. Levinger, D. Ray, M. L. Alexander and W. C. Lineberger: J. Chem. Phys. **89** (1988) 5654.
15) T. Nagata and T. Kondow: J. Chem. Phys. **98** (1993) 290.
16) T. Ikegami, T. Kondow and S. Iwata: J. Chem. Phys. **98** (1993) 3038.
17) P. J. Kuntz and J. Valldorf: Z. Phys. D **8** (1988) 195.
18) K. Hiraoka and T. Mori: J. Chem. Phys. **90** (1989) 7143.